Origin of interannual variability in global mean sea level

Benjamin D. Hamlington[a,1], Christopher G. Piecuch[b], John T. Reager[a], Hrishi Chandanpurkar[a], Thomas Frederikse[a], R. Steven Nerem[c], John T. Fasullo[d], and Se-Hyeon Cheon[e]

[a]Jet Propulsion Laboratory, California Institute of Technology, Pasadena, CA 91109; [b]Department of Physical Oceanography, Woods Hole Oceanographic Institution, Woods Hole, MA 02543; [c]Smead Aerospace Engineering Sciences, Colorado Center for Astrodynamics Research, University of Colorado, Boulder, CO 80309; [d]Climate and Global Dynamics Laboratory, National Center for Atmospheric Research, Boulder, CO 80301; and [e]Ocean, Earth, and Atmospheric Sciences Department, Old Dominion University, Norfolk, VA 23529

Edited by Anny Cazenave, Centre National d'Etudes Spatiales, Toulouse, France, and approved April 22, 2020 (received for review December 17, 2019)

The two dominant drivers of the global mean sea level (GMSL) variability at interannual timescales are steric changes due to changes in ocean heat content and barystatic changes due to the exchange of water mass between land and ocean. With Gravity Recovery and Climate Experiment (GRACE) satellites and Argo profiling floats, it has been possible to measure the relative steric and barystatic contributions to GMSL since 2004. While efforts to "close the GMSL budget" with satellite altimetry and other observing systems have been largely successful with regards to trends, the short time period covered by these records prohibits a full understanding of the drivers of interannual to decadal variability in GMSL. One particular area of focus is the link between variations in the El Niño–Southern Oscillation (ENSO) and GMSL. Recent literature disagrees on the relative importance of steric and barystatic contributions to interannual to decadal variability in GMSL. Here, we use a multivariate data analysis technique to estimate variability in barystatic and steric contributions to GMSL back to 1982. These independent estimates explain most of the observed interannual variability in satellite altimeter-measured GMSL. Both processes, which are highly correlated with ENSO variations, contribute about equally to observed interannual GMSL variability. A theoretical scaling analysis corroborates the observational results. The improved understanding of the origins of interannual variability in GMSL has important implications for our understanding of long-term trends in sea level, the hydrological cycle, and the planet's radiation imbalance.

sea level | climate variability | global mean sea level | satellite altimetry

Since 1992, satellite altimetry has provided continuous and near-global measurements of sea level, leading to the first definitive assessment of changes in global mean sea level (GMSL) (1). From the now 27-y record of satellite-measured sea level, it is estimated that GMSL is rising at a rate of ∼3 mm/y, and there are indications of an acceleration in this rise during the record (2). Although the long-term trend is a critical indicator of our warming climate, providing an integrated measure of changes across the climate system, the fluctuations that occur about this trend are also informative. The two dominant drivers of the GMSL variability at interannual to decadal timescales are steric changes due to changes in ocean heat content and barystatic changes due to the exchange of water mass between land and ocean (3, 4). With Gravity Recovery and Climate Experiment (GRACE) satellites and Argo profiling floats, it has been possible to measure the relative steric and barystatic contributions to GMSL since 2004 (5, 6). Subsequent efforts to close the budget of GMSL by comparing the combined steric and barystatic contributions to GMSL measured by satellite altimeters over the same time period (7–10) have been largely successful, particularly when focusing on trends, but the short time period covered by these records prohibits a full understanding of the drivers of interannual to decadal variability in GMSL.

Understanding the nature of this shorter-term variability and the associated GMSL response can provide important information on the impact of large-scale signals like the El Niño–Southern Oscillation (ENSO) on the global climate system (11–13), including Earth's energy budget and the global hydrological cycle. The global oceans play a dominant role in Earth's energy budget and hydrological cycle, accounting for over 90% of the changes in global heat storage, and reflecting variability in the transfer of water to and from land. Closing the GMSL budget across timescales is thus essential to closing the global energy and hydrological budgets. Perhaps most importantly from a climate change perspective, shorter-term variability serves to obscure the background trend in the still relatively short modern sea level records that are available (14–16). Improving the understanding and removing the natural fluctuations on shorter timescales could, in turn, improve our ability to detect the background forced or anthropogenic trend in GMSL. In addition, understanding the drivers of the short-term swings that occur about the long-term trend would aid in planning efforts as high-tide flooding at the coast continues to increase (e.g., ref. 17).

Despite its importance and likely due to the availability of only short records, recent literature has disagreed on the relative importance of steric and barystatic contributions to interannual variability in GMSL (18–23). Here, we attempt to provide a

Significance

Extended records of global mean steric and barystatic sea level are produced and exhibit strong agreement with satellite altimeter-observed global mean sea level (GMSL). The GMSL contributions derived from these datasets show that there are correlated steric and barystatic GMSL contributions of similar magnitudes. These variations are closely related to the El Niño–Southern Oscillation (ENSO) and provide observational support for past studies indicating important steric and barystatic GMSL contributions associated with ENSO. The improved understanding of the origins of interannual variability in GMSL established here has important implications for our understanding of long-term trends in sea level, the hydrological cycle, and the planet's radiation imbalance.

Author contributions: B.D.H., C.G.P., J.T.R., H.C., T.F., R.S.N., and J.T.F. designed research; B.D.H., C.G.P., H.C., T.F., and S.-H.C. performed research; B.D.H. contributed new reagents/analytic tools; B.D.H., C.G.P., J.T.R., H.C., T.F., R.S.N., J.T.F., and S.-H.C. analyzed data; and B.D.H., C.G.P., and T.F. wrote the paper.

The authors declare no competing interest.

This article is a PNAS Direct Submission.

Data deposition: The extended TWS dataset is available at https://figshare.com/articles/TWS_extension_mat/11971866/1. The steric sea level dataset is available at https://figshare.com/articles/Steric_Sea_Level/11971860/1.

[1]To whom correspondence may be addressed. Email: benjamin.d.hamlington@jpl.nasa.gov.

This article contains supporting information online at https://www.pnas.org/lookup/suppl/doi:10.1073/pnas.1922190117/-/DCSupplemental.

First published June 8, 2020.

clearer understanding of this variability by applying a multivariate data analysis technique to estimate variability in barystatic and steric contributions to GMSL back to 1982. These longer independent estimates allow us to investigate the observed interannual variability in satellite altimeter-measured GMSL, and understand the role of ENSO in driving changes in GMSL. We interpret our observational results in light of a simple theoretical scaling analysis, thereby improving our process-based understanding of the origin of interannual variability in GMSL.

Extending Sea Level Data Records

The GRACE record of mass change and Argo record of steric sea level are too short to yield a significant advance on the current understanding of interannual to decadal fluctuations in GMSL. We extend these records in time by applying a multivariate data analysis technique, which relies on overlapping physically related, correlated datasets with longer records. Further details can be found in *Methods*, but a brief summary is provided here for the case of extending the GRACE record. A schematic outlining the technique is also provided (Fig. 1) and connected to the explanation below.

For the purposes of this study, one of the measurements we are extending is terrestrial water storage (TWS), as measured by GRACE (representing the target variable [TV] in Fig. 1, step 1). After removing ice-related trends in the GRACE record and only using the data over land, the remaining mass changes are predominantly reflective of changes in the storage of water over land, and are highly correlated with land precipitation and land surface temperature (24). TWS is informative of barystatic sea level (25). By conservation of mass, the spatial integral of mass anomalies over all land, divided by the ocean surface area, will mirror (be equal and opposite to) anomalous barystatic sea level. Using a modern record (GRACE) and a longer, overlapping record (e.g., precipitation, or the predictor variable [PV] in Fig. 1, step 1), we compute combined statistical empirical orthogonal function (EOF)-based modes (26, 27) of variability of both datasets during the overlapping period, creating spatial patterns of the individual datasets, and a common time series of their temporal evolution (Fig. 1, step 2). We then project the spatial patterns of precipitation obtained in the EOF-based decomposition back onto the full precipitation dataset to obtain the temporal evolution of each pattern over the full length of the precipitation record (Fig. 1, step 3). Finally, we recombine the spatial patterns of GRACE from the EOF-based decomposition with the longer time series from the projection onto the precipitation data (Fig. 1, step 4). Other datasets can be used, and their inclusion has been evaluated (see *Methods*), and, in this case, the TWS extension relies on precipitation (28) and surface temperature, while the steric sea level extension uses only sea surface temperature (SST) (29). The justification for using only SST to extend steric sea level comes partially from a recent study that used SST to reconstruct historical ocean heat content back to 1871 (30). The argument made in the study is that variability in ocean heat content will be inherited at the surface and thus reflected in measurements of SST. Assuming the extension or reconstruction technique can properly account for any time lag between a change in SST and change in ocean heat content, establishing a relationship with SST should be sufficient to reproduce steric sea level changes. Additionally, the magnitude of the changes in steric sea level stem from the Argo basis functions, and the SST is used only to reproduce the temporal evolution of the basis functions back through time. Finally, the focus here is on the global mean steric sea level changes, which have been shown to be primarily controlled on these timescales by regional steric sea level changes in the tropical Pacific (18), a region where sea level and SST are strongly correlated. While not the focus of this study, extended regional steric sea level time

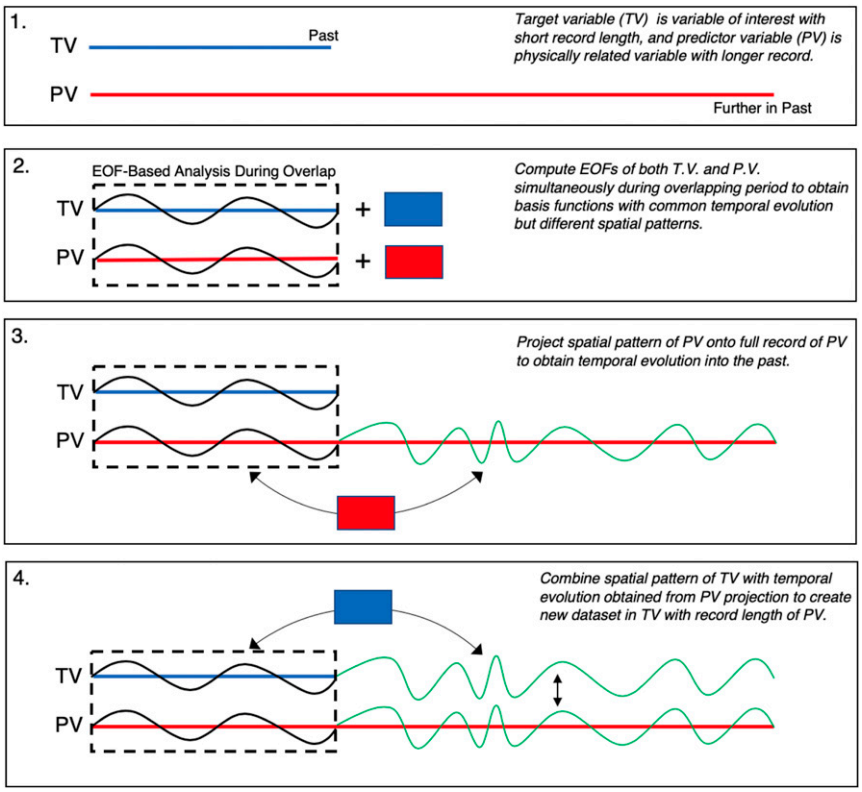

Fig. 1. Schematic showing the four steps of the data extension of a TV using a physically related PV.

series reconstructed from SST could show important systematic errors and should be treated cautiously.

The result of this procedure in this study is a half-degree, monthly TWS dataset from 1982 through 2018 (31), and a one-degree, monthly steric sea level dataset from 1982 through 2018 (32). We compute the barystatic contribution to GMSL by inverting TWS anomalies in our extended dataset and converting them to sea level change units by dividing by ocean surface area. We use the term "steric" to refer to the dataset produced here, as no attempt has been made to remove halosteric-related sea level variability, but we note that the steric contributions in GMSL are necessarily thermosteric in nature (3).

Steric and Barystatic Contributions to GMSL

To check the ability of the extended datasets to explain variations in GMSL, the barystatic and steric GMSL contributions are estimated and compared to their underlying modern data record. The extended steric dataset matches closely with the GMSL computed from the Argo dataset, showing an initial negative trend in the first half of the record before reversing in the second half (Fig. 2, *Top*). Over the full length of the extended record, there is a large increase in the steric contribution to GMSL for both the 1997/1998 and 1982/1983 El Niños. Another notable feature is a brief decline in GMSL starting in 1988 and recovering in 1990. Similarly, the barystatic contribution from the extended TWS dataset agrees well with the underlying GRACE dataset, reproducing the large increase in 2011 and the decrease that peaks in 2016 (Fig. 2, *Middle*). Prior to the GRACE record, decreases in barystatic GMSL coincide with the 1997/1998 and 1982/1983 El Niños. These extended records strengthen the conclusions in Piecuch and Quinn (18), Dieng et al. (23), and Fasullo and Nerem (34), which were either limited to short records (18, 23) or used a strictly model-based approach (34). Specifically, those studies and the analysis here suggest that ENSO variability elicits significant and near-equal magnitude in both barystatic and steric contributions to GMSL. The correlation between the barystatic and steric time series and the Multivariate ENSO Index (35) are found to be 0.53 and 0.67 from 1982 to 2018, similar to the correlations obtained by Piecuch and Quinn (18) from 2005 to 2015.

We also note that steric and barystatic GMSL time series can be computed from other available datasets. *SI Appendix*, Fig. S1 provides a comparison of several steric sea level GMSL time series, including the one produced here. There is little agreement between the different time series, which generally have very large amplitude interannual variability throughout the record. For the barystatic GMSL contribution, a comparison is made between the presently extended dataset and the reconstruction of Humphrey and Gudmundsson (25). (*SI Appendix*, Fig. S2). The two time series agree well during the GRACE time period, but diverge as the record is extended into the past. The reason for this divergence is not immediately clear, and requires a more in-depth examination to determine which one may be more representative of barystatic sea level. Furthermore, in a recent study, global hydrological models were shown to not reproduce the interannual to decadal variability in the GRACE record, concluding that the models are not suitable to quantify global TWS-induced barystatic changes prior to the GRACE record (36). As a result of these differences, associated studies, and the fact that fully assessing the origin of these disagreements is outside of the scope of the paper, the rest of the paper only considers and uses the datasets produced here.

The steric and barystatic GMSL contribution time series can be combined and then compared to total sea level as measured by satellite altimeters (Fig. 2, *Bottom*; description of altimeter data in *Methods*). To quantify the consistency and agreement between time series, the percentage of variance in the GMSL time series that is explained by the steric, barystatic, and combined contributions is computed over different time periods (Table 1). For each time period, the variance explained by the

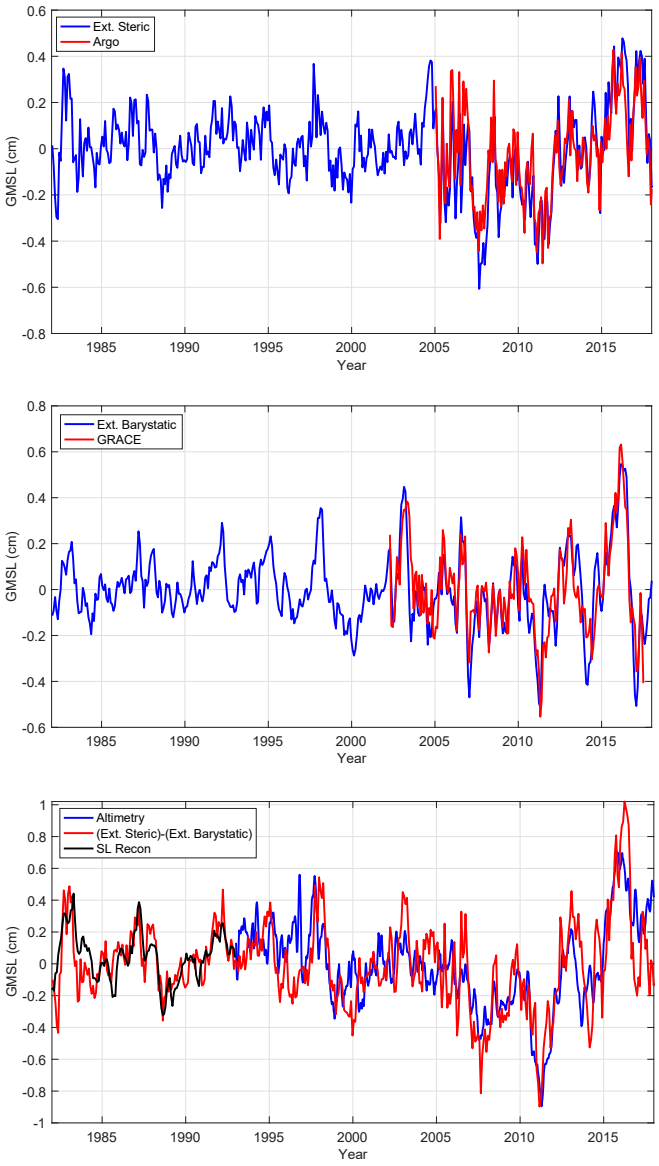

Fig. 2. (*Top*) Steric contribution to GMSL from 1982 to 2018 estimated from extended dataset and Argo measurements. (*Middle*) Barystatic contribution to GMSL from 1982 to 2018 estimated from extended TWS dataset and GRACE data. (*Bottom*) Comparison of combination of steric and barystatic contributions from extended datasets to satellite altimetry and a sea level reconstruction.

steric time series alone is greater than 65%, while the variance explained by the barystatic time series is greater than 42% (note that the explained variance is defined here as the percentage difference between the variance in total GMSL and variance in GMSL minus the contributor time series). Most importantly, the combination of the two contributors explains more than 76% of the variance in the altimeter-measured GMSL for each time period. The rms value of the residuals between the altimetry GMSL and combined steric and barystatic contributions is also less than 2 mm. In general, the residuals are small (<2 mm) throughout the record, except during two time periods: 1996/1997 and 2016/2017. The causes of these discrepancies remain to be understood. While a formal error analysis is beyond the scope of the present study (discussed in more detail below), Piecuch and Quinn (18) provide SE estimates in the range of 1 mm to 2 mm for monthly Argo, GRACE, and altimetry GMSL time

Table 1. Percentage of explained variance of altimetry GMSL time series for steric, barystatic, and combined contributions for different time periods

	2005–2019, %	1993–2019, %	1982–2019, %
Steric	73	65	65
Barystatic	43	42	45
Steric + barystatic	83	76	77

For the period from 1982 to 2019, the sea level reconstruction is used prior to 1993. A 12-mo smoothing is also applied to each time series prior to computing the explained variance.

series. This serves as a baseline for the uncertainties on the products generated here. In terms of specific events within the record, both the altimetry and combined contributors have an increase of ∼0.5 cm associated with the 1997/1998 El Niño. To provide a comparison prior to the altimeter record, a reconstruction of sea level that combines tide gauges and satellite altimetry can be used (33) (Fig. 2, *Bottom*, black). The combined extended datasets reproduce the decline in GMSL from 1988 to 1990, and the increase in GMSL associated with the 1982/1983 El Niño. While other sea level reconstructions have been produced and often disagree, Chambers et al. (37), Calafat et al. (38), and Dangendorf et al. (39) all reconstruct the almost ∼1-cm decline in GMSL that starts in 1988. Chambers et al. (37) examined this event in greater detail, finding agreement with sea level measurements made by Geosat. Comparing the reconstruction used here and the reconstruction from Calafat et al. (38) shows the general agreement between reconstruction products (*SI Appendix*, Fig. S3). Also, to test the sensitivity of these comparisons to the underlying datasets, we have repeated

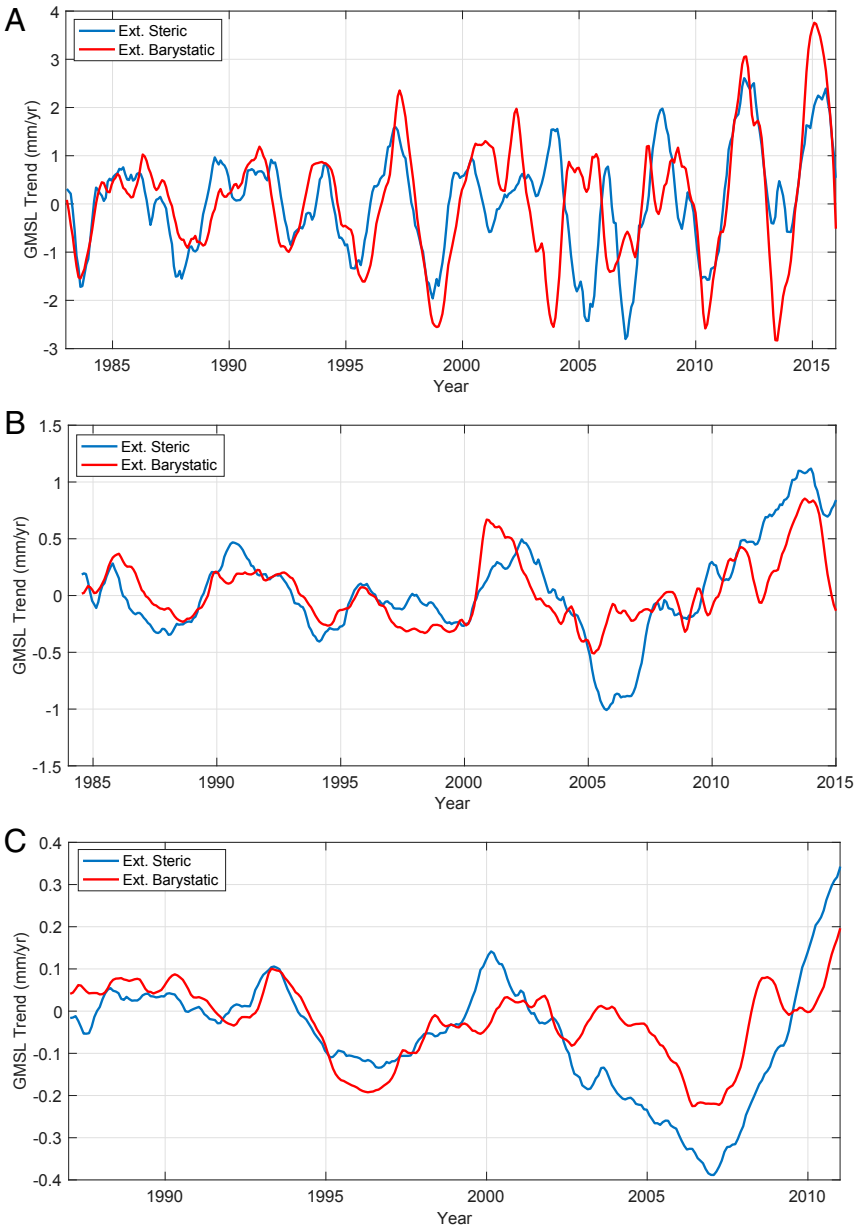

Fig. 3. Short-term trends in the steric and barystatic contributions to GMSL from the extended datasets, computed using a (*A*) 2-y window, (*B*) 5-y window, and (*C*) 10-y window.

the analysis using precipitation, surface temperature, and SST from the National Centers for Environmental Prediction reanalysis (40) The resulting correlations are provided in *SI Appendix*, Table S1, and demonstrate that similar conclusions can be drawn when relying on different datasets for the PVs.

We now examine relative steric and barystatic contributions to GMSL over different timescales. To do this, we compute running 2-, 5-, and 10-y trends from the GMSL time series covering the time period from 1982 to 2018 (Fig. 3). The 2- and 5-y trends are chosen to be representative of the timescales upon which ENSO typically varies, and the 10-y trends are selected to focus on decadal variability in GMSL. For the 2-y trends that are most representative of interannual variability, the barystatic contribution is as large as the steric contribution and appears to increase in magnitude toward the end of the record. Consistent with the comparisons made in Fig. 2 and discussed above, the steric and barystatic trends are of similar sign and magnitude for most of the record, particularly during significant ENSO events. The steric contribution appears to lead (by a couple of months) the barystatic contribution for several of these events (e.g., 1982/1983, 2009/2010, and 2015/2016 El Niños and 1988/1989 and 2010/2011 La Niñas), supporting the findings of ref. 34. Short-term trends can still be large during non-ENSO events. At longer timescales, the steric contribution begins to exceed the barystatic contribution, particularly for the 10-y trends (Fig. 3*C*). Both the steric and barystatic 5- and 10-y trends are large and mostly correlated during the record, highlighting the role of enhancing or suppressing the background trend in GMSL depending on the time period of interest, consistent with recent studies (e.g., ref. 24).

Scaling Analysis of GMSL Contributions

Based on the analysis conducted above, there are three key findings regarding the relative contributions to variations in GMSL, particularly on interannual timescales: 1) Barystatic and steric contributions are nearly equal in magnitude, 2) the barystatic and steric contributions are generally correlated, and 3) both contributions are strongly connected to variations in ENSO. This result, obtained over a longer time period than other comparable previous studies, provides strong support for the results of refs. 18, 23, and 34, while disagreeing with the assessment that changes in GMSL are mostly driven by barystatic variability (12, 21, 22). It remains to determine whether there is a physical explanation for why the barystatic and steric GMSL contributions are generally correlated and of similar magnitude. To generate an initial hypothesis, we consider the changes in air–sea exchanges on interannual to decadal timescales. While the intent here is for the analysis to apply in general, the ENSO-related behavior and response is of particular focus. By conservation of volume, changes in barystatic sea level (η_F) can only be driven by anomalous air–sea freshwater flux,

$$\frac{\partial \eta_F}{\partial t} = \frac{1}{A}\iint_A \frac{1}{\rho_0}(E + P + R)dA, \qquad [1]$$

where E, P, and R are evaporation, precipitation, and runoff, respectively, ρ_0 is a reference ocean density, and A is the global ocean surface area. We assume that the change in global mean steric sea level (η_Q) is given by

$$\frac{\partial \eta_Q}{\partial t} = \frac{1}{A}\iint_A \frac{\alpha}{\rho_0 c_p}(Q_E + Q_H + Q_L + Q_S)dA, \qquad [2]$$

where α is the thermal expansion coefficient, c_p is the specific heat capacity of seawater, and Q_E, Q_H, Q_L, and Q_S are the latent, sensible, longwave, and shortwave fluxes, respectively. This assumption neglects any (probably higher-order) contributions from internal redistribution by ocean currents and nonlinearities in the seawater equation of state. As discussed in a recent study (41), anomalous latent evaporative heat fluxes are an important driver of heat flux in the tropical Pacific on interannual and longer timescales (see *SI Appendix*, Fig. S4 for further support). Those heat fluxes are proportional to anomalous evaporation, such that the ocean will lose water mass through evaporation at the same time evaporative cooling occurs, or

$$Q_E = \Lambda \mathrm{E}, \qquad [3]$$

where Λ is the latent heat of vaporization of seawater. This anomalous evaporation will be offset, in part, by precipitation. In other words, the increased evaporation will lead to increased precipitation. Using observational precipitation data (see TWS Dataset), in general, 25% of this increased precipitation will fall over land. This percentage ranges from ~20 to 30% for El Niño and La Niña, respectively (*SI Appendix*, Fig. S5). Scaling the barystatic contribution by this percentage, the relative contributions of barystatic and steric variability can be given in terms of Eqs. **1** and **2**,

$$\frac{\partial \eta_F / \partial t}{\partial \eta_Q / \partial t} \approx \frac{0.25 c_p}{\alpha \Lambda} \approx 1, \qquad [4]$$

where we assume representative values for the constants of $c_p \approx 4\times10^3$ J·kg^{-1}·°C^{-1}, $\Lambda \approx 2.5\times10^6$ J·kg^{-1}, and $\alpha \approx 3\times10^{-4}$ °C^{-1} (assumed reasonable for the tropical ocean). While future studies will examine the impact of the assumptions made and further investigate the relevant driving mechanisms, this preliminary analysis provides a potential lowest-order physical explanation for the observation-based results presented in this paper. Specifically, both approaches show that steric and barystatic GMSL changes in response to ENSO-like conditions are correlated and of similar magnitude. On the shorter timescales (Fig. 3*A*), the scaling between the two contributors in Eq. **3** appears representative of the observations, with TWS contributions generally exceeding steric contributions. This appears less true on longer timescales, but a more thorough examination of the physical drivers is required before drawing further conclusions.

Discussion

There are a couple of caveats and potential limitations to consider when interpreting the results presented above. First, the overlapping period for the steric and TWS datasets is limited to 15 y, raising questions regarding the ability to capture decadal variability. Any partial cycle of longer-timescale variability will still be represented in the EOF-based modes, and thus will be imparted on the resulting extended dataset. It is difficult to assess the degree to which this variability is represented, so we note it as a limitation of the technique, focus largely on the interannual timescale, and adjust our conclusions accordingly. Second, uncertainty in the extended datasets is a function of several factors. These factors include length of the overlapping time period (discussed above), representativeness of the modes computed during the overlapping time period to the full record, number of EOF-based modes used in the procedure, uncertainty in the TV datasets, uncertainty in the PV datasets, and choice of the PV datasets. The uncertainty associated with the latter three factors is testable, but leads to likely unrealistically small error estimates in terms of global mean contributions. Recognizing the potential limitation in our ability to fully assess the uncertainty, the analysis we perform here is focused primarily on scaling analyses, and we specifically avoid attempting any type of "budget closure" exercise. Finally, in an attempt to test the ability of the procedure outlined above to extend the datasets

back in time, we have used a model large ensemble (LENS)–the Community Earth System Model (CESM) to conduct sensitivity testing (see *Methods* and *SI Appendix*, Fig. S6). The goal of this sensitivity testing is simply to determine whether physically related predictor datasets can be used to extend the record of a TV back in time. There are model biases and uncertainties that could impact these results, but choose to still include the results of the test as an additional piece of support for the procedure implemented here.

By extending the records of steric sea level and TWS over a longer time period, advances in our understanding of the variability in GMSL have been demonstrated in this paper. On a basic level, the strong agreement between the GMSL contributions estimated from the extended steric and TWS datasets, the satellite altimetry data, and the tide gauge reconstructions serves as validation for each dataset. In terms of the information derived from these datasets, we have shown that there are correlated barystatic and steric GMSL contributions of similar magnitudes in response to ENSO variability from 1982 to 2018, supporting refs. 18, 23, and 34 but disagreeing with refs. 12, 21, and 22. Based on the results contained herein and with longer records of TWS and steric sea level, there are many other avenues of study to pursue. The relative steric and barystatic contributions to variability in GMSL have potentially important implications for the understanding of Earth's energy budget and the hydrological cycle that need to be investigated in light of the budget analysis performed here. For example, quantifying the Earth energy imbalance is typically done using Argo-based estimates, which vary across products. The extended datasets produced here along with the good agreement demonstrated in Table 1 potentially provide a further avenue for study. Furthermore, regional patterns of steric sea level and TWS are provided by the extended datasets, and can shed light on the regional responses to climate signals like ENSO. Finally, the role of interannual to decadal variability in obscuring the background trend in GMSL was mentioned earlier in the paper. With the demonstrated consistency between the different datasets, particularly on interannual timescales, it may be possible to remove the GMSL variations associated with one or both of the contributors from the satellite altimeter record and reexamine the underlying trend and acceleration (e.g., ref. 2). In short, although the focus here is on interannual to decadal variability, the analysis and the opportunity presented by longer records can lead to an improved understanding of changes in sea level across a large range of timescales.

Methods

Data Extension Method. The premise of the data extension technique used here originates from Smith et al. (42), with further refinement in Hamlington et al. (43). Specifically, those studies demonstrated that a particular TV can be reconstructed or extended back in time by relying on statistical relationships to other climate variables with longer observational records. While both reconstructed the TV (precipitation and sea level, respectively) back to the beginning of the 20th century, here the records are only extended back to the beginning of the 1980s. Smith et al. (42) used canonical correlation analysis to establish relationships between the TVs and extending variables, and Hamlington et al. (44) used a combination of cyclostationary EOFs (CSEOFs) (44) and a simple regression technique. Here, a modified procedure is used and described as follows.

1) Identify a modern record to serve as the TV (e.g., TWS from GRACE) and a PV that is physically related but has a longer, overlapping record (e.g., precipitation).
2) Compute combined CSEOF modes of variability of TV and PV during the overlapping period, creating spatial patterns with common temporal evolution. In other words, each returned mode contains two spatial patterns (one for TV and one for PV), and a single time series representing the spatial evolution.
3) Project the spatial patterns of PV obtained in step 1 back onto the full record of PV to obtain the temporal evolution of each pattern over the length of PV.
4) Recombine the spatial patterns of TV obtained in step 1 with the time series obtained in step 2.

The result of this procedure is a dataset in the variable of TV with the record length of PV. Note, more than one variable can be included as PV in this procedure. The seasonal cycle is included in this procedure, although is removed prior to the analysis conducted here. The trend is dealt with differently for the steric and TWS extended datasets, discussed in more detail below.

It should be noted that CSEOFs play an important role in this procedure. Prior to computing CSEOFs, a specific nested period is chosen for the returned modes (the details on the selection of this nested period can be found in ref. 44). The spatial patterns of each mode thus have a periodicity imposed by the chosen nested period. For example, for the case of an annual cycle that is present in a dataset with monthly temporal resolution, each mode will contain 12 spatial patterns (one for each month) and an associated time series that represents the amplitude variations of the annual cycle. The relaxing of the stationarity requirement when compared to traditional EOFs is critical for the procedure described above. Variations associated with the seasonal cycle in precipitation are known to lead variations in TWS, with the associated time lags differing across the globe. CSEOFs as computed in step 1 can capture this lagged relationship in addition to the spatial variability in this relationship across the globe. As long as the lag between variables is less than the chosen nested period, CSEOFs provide the opportunity to capture the relationship in a single mode. In other words, the procedure developed and used here does require included variables to be in phase and/or correlated.

Steric Sea Level Dataset. The steric sea level dataset produced here uses a gridded Argo dataset from 2005 through 2017 as the TV, and SST from the Optimum Interpolation Sea Surface Temperature (OISST v2) (56) from 1982 to present as the extending variable (PV). The start date of this dataset sets the start date of the analysis performed here. Prior to computing the combined CSEOFs, no editing is performed, and the spatial pattern of the trends in the final dataset is preserved. To compute the gridded steric sea level dataset from Argo, we used monthly Argo in situ temperature and salinity distributed by the Scripps Institution of Oceanography. The resolution of the data are a half-degree over 65°S to 65°N, and the depth from the surface to 2,000 m is divided into 58 sections with different increments (coarser grid for deeper depth). Steric sea level is then computed following Gill and Niiler (45). It should be noted that there is some disagreement between different datasets generated using the in situ Argo measurements, and these differences are even more dramatic when attempting to extend the record of steric sea level prior to 2005. The steric contribution to GMSL is shown for several of these datasets, in *SI Appendix*, Fig. S1, along with GMSL from the dataset generated as part of this study. Due to the substantial differences and the fact that the other products are unable to approach the satellite altimetry GMSL when combined with the TWS contribution, we only consider the steric product generated here in the main paper.

TWS Dataset. For the TWS dataset, we use monthly gridded estimates of equivalent water thickness based on retrievals from GRACE. Specifically, we used the mascon solutions from Release-06 data generated by the NASA Jet Propulsion Laboratory (JPL) (46, 47) The data, whose native resolution is about 200,000 km^2, are regridded at 0.5° spatial resolution and covers the time period from April 2002 through end of mission (June 2017). While GRACE also provides measurements over the ocean and the ice sheets, only data over land are used here to focus on TWS. Several monthly gaps in the dataset were filled with interpolation relying on classical decomposition that uses information about the trend, seasonal cycle, and residual variability about these signals. To establish the statistical relationship with GRACE and extend the record into the past, we use precipitation measurements from the Global Precipitation Climatology Project (v2.3) (48) dataset covering the time period from 1979 to present, in addition to the 2-m temperature from ERA5 (49) covering the same time period. Prior to use, both datasets were regridded to the same grid as the GRACE data. As with the GRACE data, we again use only the observations over land. Since the focus here is on the variability about the trends, the trends over ice-covered regions are removed prior to analysis. While other trends are retained, precipitation and 2-m temperature data unlikely to be representative of some of the trends in the GRACE dataset (e.g., trends associated with groundwater withdrawal), and resulting trends on a regional level, should be treated with caution.

Altimetry Data. Similar to ref. 8, we choose not to rely on a single satellite altimetry-derived GMSL time series. Instead, we use the ensemble average from five groups: AVISO (50), Colorado (51), CSIRO (52), NOAA (53), and JPL (54). The time series are interpolated onto regular monthly intervals from 1993 through 2018 prior to use.

Sensitivity Testing. Validation of the extended steric and TWS datasets is a challenge given the lack of available TWS observations prior to GRACE, and the disagreement between steric sea level products prior to Argo (*SI Appendix*, Fig. S1). In an attempt to test the ability of the procedure outlined above to extend the datasets back in time, we use a model LENS–CESM (55). Specifically, we take precipitation, TWS, surface temperature, SST, and steric sea level fields from LENS and repeat the extension procedure. We take length segments (37 y) equivalent to those provided by the actual observations, and extract the last 13 y to use in step 1 of the procedure above. Once the extended datasets are created, we can compare the result to the "truth" provided by the modeled TWS and steric sea level. Due to computational constraints, this procedure is repeated 100 times for both steric and TWS datasets. The results of these tests are shown in *SI Appendix*, Fig. S6, showing only the correlation between the extended GMSL contribution and the actual contribution for steric (with annual cycle, *SI Appendix*, Fig. S6*A*, and without annual cycle, *SI Appendix*, Fig. S6*B*) and barystatic (SI Appendix, Fig. S6 *C* and *D*). While providing some indication of ability to extend the datasets using the procedure presented here, it should be noted that there are differences between the model and observations that could impact the results. One, in particular, is that the CSEOF analysis of LENS returns an annual mode that explains more of the overall variance when compared to the annual mode from the observations. This increase in explained variance appears to come at the cost of explained variance in the ENSO-related modes. A further investigation is beyond the scope of this study, but the results of the sensitivity test are included here as a preliminary check on the quality of the datasets used.

Data Availability Statement. The extended TWS dataset is available at https://figshare.com/articles/TWS_extension_mat/11971866/1. The steric sea level dataset is available at https://figshare.com/articles/Steric_Sea_Level/11971860/1. Gridded Surface Height Anomalies Version 1801, Ver. 1801 is available from NASA JPL Physical Oceanography Distributed Active Archive Center at http://dx.doi.org/10.5067/SLREF-CDRV1.

ACKNOWLEDGMENTS. The research was carried out at JPL, California Institute of Technology, under a contract with NASA. This study was funded by NASA Grants NNX17AH35G (Ocean Surface Topography Science Team), 80NSSC17K0564, and 80NSSC17K0565 (NASA Sea Level Change Team). The efforts of J.T.F. in this work were also supported by NSF Award AGS-1419571, and by the Regional and Global Model Analysis component of the Earth and Environmental System Modeling Program of the US Department of Energy's Office of Biological & Environmental Research via National Science Foundation Grant IA 1844590. C.G.P. was supported by the J. Lamar Worzel Assistant Scientist Fund and the Penzance Endowed Fund in Support of Assistant Scientists at the Woods Hole Oceanographic Institution.

1. R. S. Nerem, D. P. Chambers, C. Choe, G. T. Mitchum, Estimating mean sea level change from the TOPEX and Jason altimeter missions. *Mar. Geod.* **33**, 435–446 (2010).
2. R. S. Nerem *et al.*, Climate-change-driven accelerated sea-level rise detected in the altimeter era. *Proc. Natl. Acad. Sci. U.S.A.* **115**, 2022–2025 (2018).
3. J. M. Gregory *et al.*, Concepts and terminology for sea level: Mean, variability and change, both local and global. *Surv. Geophys.* **40**, 1291–1292 (2019).
4. J. A. Church *et al.*, *Sea Level Change*, (Cambridge University Press, 2013).
5. D. P. Chambers, J. Wahr, R. S. Nerem, Preliminary observations of global ocean mass variations with GRACE. *Geophys. Res. Lett.* **31**, L13310 (2004).
6. D. Roemmich, J. Gilson, The 2004–2008 mean and annual cycle of temperature, salinity, and steric height in the global ocean from the Argo Program. *Prog. Oceanogr.* **82**, 81–100 (2009).
7. E. W. Leuliette, L. Miller, Closing the sea level rise budget with altimetry, Argo, and GRACE. *Geophys. Res. Lett.* **36** (2009).
8. E. W. Leuliette, J. K. Willis, Balancing the sea level budget. *Oceanography (Wash. D.C.)* **24**, 122–129 (2011).
9. E. W. Leuliette, The balancing of the sea-level budget. *Curr. Clim. Change Rep.* **1**, 185–191 (2015).
10. WCRP Global Sea Level Budget Group, Global sea-level budget 1993–present. *Earth Syst. Sci. Data* **10**, 1551–1590 (2018).
11. R. S. Nerem, D. P. Chambers, E. W. Leuliette, G. T. Mitchum, B. S. Giese, Variations in global mean sea level associated with the 1997–1998 ENSO event: Implications for measuring long term sea level change. *Geophys. Res. Lett.* **26**, 3005–3008 (1999).
12. A. Cazenave *et al.*, Estimating ENSO influence on the global mean sea level, 1993–2010. *Mar. Geod.* **35**, 82–97 (2012).
13. W. Han *et al.*, "Spatial patterns of sea level variability associated with natural internal climate modes" in *Integrative Study of the Mean Sea Level and Its Components*, A. Cazenave, N. Champollion, F. Paul, J. Benveniste, Eds. (Springer, Cham, Switzerland, 2017), pp. 221–254.
14. B. D. Hamlington, J. T. Fasullo, R. S. Nerem, K. Y. Kim, F. W. Landerer, Uncovering the pattern of forced sea level rise in the satellite altimeter record. *Geophys. Res. Lett.* **46**, 4844–4853 (2019).
15. B. D. Hamlington *et al.*, Uncovering an anthropogenic sea-level rise signal in the Pacific Ocean. *Nat. Clim. Chang.* **4**, 782–785 (2014).
16. X. Zhang, J. A. Church, Sea level trends, interannual and decadal variability in the Pacific Ocean. *Geophys. Res. Lett.* **39**, L21701 (2012).
17. A. G. Burgos, B. D. Hamlington, P. R. Thompson, R. D. Ray, Future nuisance flooding in Norfolk, VA, from astronomical tides and annual to decadal internal climate variability. *Geophys. Res. Lett.* **45**, 12–432 (2018).
18. C. G. Piecuch, K. J. Quinn, El Niño, La Niña, and the global sea level budget. *Ocean Sci.* **12**, 1165–1177 (2016).
19. J. T. Fasullo, C. Boening, F. W. Landerer, R. S. Nerem, Australia's unique influence on global sea level in 2010–2011. *Geophys. Res. Lett.* **40**, 4368–4373 (2013).
20. C. Boening, J. K. Willis, F. W. Landerer, R. S. Nerem, J. Fasullo, The 2011 La Niña: So strong, the oceans fell. *Geophys. Res. Lett.* **39**, L19602 (2012).
21. W. Llovel *et al.*, Terrestrial waters and sea level variations on interannual time scale. *Global Planet. Change* **75**, 76–82 (2011).
22. A. Cazenave *et al.*, The rate of sea-level rise. *Nat. Clim. Chang.* **4**, 358–361 (2014).
23. H. B. Dieng *et al.*, Effect of La Niña on the global mean sea level and North Pacifc Ocean mass over 2005-2011. *J. Geod. Sci.* **4**, 19–27 (2014).
24. J. T. Reager *et al.*, A decade of sea level rise slowed by climate-driven hydrology. *Science* **351**, 699–703 (2016).
25. V. Humphrey, L. Gudmundsson, GRACE-REC: A reconstruction of climate-driven water storage changes over the last century. *Earth Syst. Sci. Data* **11**, 1153–1170 (2019).
26. K. Y. Kim, B. Hamlington, H. Na, Theoretical foundation of cyclostationary EOF analysis for geophysical and climatic variables: Concepts and examples. *Earth Sci. Rev.* **150**, 201–218 (2015).
27. B. D. Hamlington *et al.*, The dominant global modes of recent internal sea level variability. *J. Geophys. Res. Oceans* **124**, 2750–2768 (2019).
28. R. F. Adler *et al.*, The Global Precipitation Climatology Project (GPCP) monthly analysis (new version 2.3) and a review of 2017 global precipitation. *Atmosphere (Basel)* **9**, 138 (2018).
29. R. W. Reynolds *et al.*, Daily high-resolution-blended analyses for sea surface temperature. *J. Climate* **20**, 5473–5496 (2007).
30. L. Zanna, S. Khatiwala, J. M. Gregory, J. Ison, P. Heimbach, Global reconstruction of historical ocean heat storage and transport. *Proc. Natl. Acad. Sci. U.S.A.* **116**, 1126–1131 (2019).
31. B. D. Hamlington, Terrestrial water storage dataset from 1982 to 2019. Figshare. https://figshare.com/articles/TWS_extension_mat/11971866/1. Deposited 11 March 2019.
32. B. D. Hamlington, Steric sea level dataset from 1982 to 2019. Figshare. https://figshare.com/articles/Steric_Sea_Level/11971860. Deposited 11 March 2019.
33. B. D. Hamlington, R. R. Leben, M. W. Strassburg, K. Y. Kim, Cyclostationary empirical orthogonal function sea-level reconstruction. *Geosci. Data J.* **1**, 13–19 (2014).
34. J. Fasullo, R. Nerem, Interannual variability in global mean sea level estimated from the CESM large and last millennium ensembles. *Water* **8**, 491 (2016).
35. K. Wolter, Multivariate ENSO Index (MEI). Climate diagnostics center report. https://www.psl.noaa.gov/enso/mei/index.html. Accessed 1 November 2019.
36. B. R. Scanlon *et al.*, Global models underestimate large decadal declining and rising water storage trends relative to GRACE satellite data. *Proc. Natl. Acad. Sci. U.S.A.* **115**, E1080–E1089 (2018).
37. D. P. Chambers, C. A. Mehlhaff, T. J. Urban, D. Fujii, R. S. Nerem, Low-frequency variations in global mean sea level: 1950–2000. *J. Geophys. Res. Oceans* **107**, 1 (2002).
38. F. M. Calafat, D. P. Chambers, M. N. Tsimplis, On the ability of global sea level reconstructions to determine trends and variability. *J. Geophys. Res. Oceans* **119**, 1572–1592 (2014).
39. S. Dangendorf *et al.*, Persistent acceleration in global sea-level rise since the 1960s. *Nat. Clim. Chang.* **9**, 705–710 (2019).
40. Kalnay *et al.*, The NCEP/NCAR 40-year reanalysis project. *Bull. Am. Meteorol. Soc.* **77**, 437–470 (1996).
41. C. G. Piecuch, P. R. Thompson, R. M. Ponte, M. A. Merrifield, B. D. Hamlington, What caused recent shifts in tropical Pacific decadal sea-level trends? *J. Geophys. Res. Oceans* **124**, 7575–7590 (2019).
42. T. M. Smith, P. A. Arkin, M. R. Sapiano, Reconstruction of near global annual precipitation using correlations with sea surface temperature and sea level pressure. *J. Geophys. Res. D Atmospheres* **114** (2009).
43. B. D. Hamlington, R. R. Leben, K. Y. Kim, Improving sea level reconstructions using non-sea level measurements. *J. Geophys. Res. Oceans* **117**, C10025 (2012).
44. K. Y. Kim, B. Hamlington, H. Na, Theoretical foundation of cyclostationary EOF analysis for geophysical and climatic variables: Concepts and examples. *Earth Sci. Rev.* **150**, 201–218 (2015).
45. A. E. Gill, P. P. Niiler, The theory of the seasonal variability in the ocean. *Deep-Sea Res. Oceanogr. Abstr.* **20**, 141–177 (1973).
46. D. N. Wiese, F. W. Landerer, M. M. Watkins, Quantifying and reducing leakage errors in the JPL RL05M GRACE mascon solution. *Water Resour. Res.* **52**, 7490–7502 (2016).

47. M. M. Watkins, D. N. Wiese, D. N. Yuan, C. Boening, F. W. Landerer, Improved methods for observing Earth's time variable mass distribution with GRACE using spherical cap mascons. *J. Geophys. Res. B Solid Earth* **120**, 2648–2671 (2015).
48. R. F. Adler *et al*., The version-2 global precipitation climatology project (GPCP) monthly precipitation analysis (1979–present). *J. Hydrometeorol.* **4**, 1147–1167 (2003).
49. Copernicus Climate Change Service, (C3S) ERA5: Fifth generation of ECMWF atmospheric reanalyses of the global climate. https://cds.climate.copernicus.eu/#!/search?text=ERA5&type=dataset. Accessed 1 November 2019.
50. M. Ablain, A. Cazenave, G. Valladeau, S. Guinehut, A new assessment of the error budget of global mean sea level rate estimated by satellite altimetry over 1993-2008. *Ocean Sci.* **5**, 193–201 (2009).
51. R. S. Nerem, D. P. Chambers, E. W. Leuliette, G. T. Mitchum, B. S. Giese, Variations in global mean sea level associated with the 1997–1998 ENSO event: Implications for measuring long term sea level change. *Geophys. Res. Lett.* **26**, 3005–3008 (1999).
52. J. A. Church, N. J. White, Sea-level rise from the late 19th to the early 21st century. *Surv. Geophys.* **32**, 585–602 (2011).
53. E. W. Leuliette, R. Scharroo, Integrating Jason-2 into a multiple-altimeter climate data record. *Mar. Geod.* **33**, 504–517 (2010).
54. V. Zlotnicki, Z. Qu, J. Willis, MEaSUREs Gridded Sea Surface Height Anomalies, Version 1812. https://doi.org/10.5067/SLREF-CDRV2. Accessed 1 August 2019.
55. J. E. Kay *et al*., The Community Earth System Model (CESM) large ensemble project: A community resource for studying climate change in the presence of internal climate variability. *Bull. Am. Meteorol. Soc.* **96**, 1333–1349 (2015).
56. R. W. Reynolds, V. F. Banzon, NOAA Optimum Interpolation 1/4 Degree Daily Sea Surface Temperature (OISST) Analysis, Version 2. https://data.nodc.noaa.gov/cgi-bin/iso?id=gov.noaa.ncdc.C00844. Accessed 1 November 2019.